Latin American Journal of Solids and Structures
www.lajss.org

Vibration suppression of a rotating flexible cantilever pipe conveying fluid using piezoelectric layers

Abstract

In this study, the governing equations of a rotating cantilever pipe conveying fluid are derived and the longitudinal and lateral induced vibrations are controlled. The pipe considered as an Euler Bernoulli beam with tip mass which piezoelectric layers attached both side of it as sensors and actuators. The follower force due to the fluid discharge causes both conservative and non-conservative work. For mathematical modeling, the Lagrange–Rayleigh–Ritz technique is utilized. An adaptive-robust control scheme is applied to suppress the vibration of the pipe. The adaptive-robust control method is robust against parameter uncertainties and disturbances. Finally, the system is simulated and the effects of varying parameters are studied. The simulation results show the excellent performance of the controller.

Keywords

Rotating flexible pipe; cantilever pipe conveying fluid; piezoelectric layers; adaptive-robust control scheme.

S. Khajehpour[a]
V. Azadi[b]

Department of Mechanical Engineering
Shiraz Branch, Islamic Azad University,
Shiraz, I. R. Iran.

Corresponding author:
[a]skhajehpour@gmail.com
[b]vahid.azd@gmail.com

http://dx.doi.org/10.1590/1679-78251535

Received 24.08.2014
In revised form 10.03.2015
Accepted 10.03.2015
Available online 10.04.2015

1 INTRODUCTION

In several partial engineering examples we can find rotating cantilever beams such as maneuvering spacecraft and aircraft engines. Reducing the induced vibration amplitudes of these structures is very important to increase the performance of them.

Fung and Yau (1999) have modeled a clamped-free rotating flexible robotic arm by Euler-Bernoulli beam theory. The arm rotated horizontally about the clamped axis while the other end was constrained to move against a curve, the arm had an end mass attached at its tip. The dynamic stability of plane transverse oscillations of two cantilevered pipes inter connected along their outer radii and conveying different fluids with different flow speeds was studied by Langthjem and Sugiyama (1999). Lim et al. (2003) have examined the vibration of a flexible cantilever tube with nonlinear constraints when it was subjected to internal flow by experimental and theoretical analysis. A numerical analysis was made of the dynamic stability of a cantilevered steel pipe conveying a

fluid by Dzhupanov and Markova (2003). The pipe was modeled by a beam restrained at the left end and supported by a special device at the other end.

Fung and Yau (2004) investigated the vibration behavior and control of a clamped-free rotating flexible cantilever arm with fully covered active constrained layer damping (ACLD) treatment. The arm was rotating in a horizontal plane in which the gravitational effect and rotary inertia were neglected.

Yoon and Son (2006) have studied the effects of the open crack and a moving mass on the dynamic behavior of a simply supported pipe conveying fluid. They also investigated the effects of a tip mass and fluid flow on the dynamic behavior of a rotating cantilever pipe conveying fluid (Yoon and Son, 2007). They did not apply any active control to suppress the pipe vibrations. The investigation of the three-dimensional nonlinear dynamics of unrestrained and restrained cantilever pipe conveying fluid was undertaken by Gagnon et al. (2007). Paidoussis et al. (2007) have investigated the three-dimensional nonlinear dynamics of a vertical cantilevered pipe conveying fluid, additionally constrained by arrays of four or two springs or a single spring at a point along its length. Using Lagrange's equations and an improved transverse displacement expansion, the non-linear free and forced vibrations of simply supported thin circular cylindrical shells were investigated by Rougui et al. (2007). Lin and Qiao (2008) have studied vibration and stability of an axially moving beam in fluid and constrained by simple supports with torsion springs. Wang et al. (2010a) studied the nonlinear traveling wave response of a cantilever circular cylindrical shell subjected to a concentrated harmonic force moving in a concentric circular path at a constant velocity. The dynamic response of a cantilever rotating circular cylindrical shell subjected to a harmonic excitation about one of the lowest natural frequency was investigated by Wang et al. (2010b). Askari and Daneshmand (2010) have considered the coupled-vibration analysis of a cantilever cylindrical shell partially submerged in a fluid with a continuous, simply connected and non-convex domain.

Optimal control of a thin-walled rotating beam was considered using a higher-order shear deformation theory by Chandiramani (2010). Rinaldi and Paidoussis (2010) are investigated the dynamics of a flexible cantilevered pipe fitted with a special end-piece.

A set of simplified boundary conditions for a flexible beam connected to a rigid body at one end and free at the other end, which was applied to the case of a fluid- conveying, fluid-immersed pipe, was presented by Hellum et al. (2011). Wang and Dai (2012) studied the vibration and stability properties of fluid-conveying pipes with two symmetric elbows fitted at downstream end. The nonlinear planar dynamics of a fluid conveying cantilevered pipe was investigated by Ghayesh et al. (2013). By modifying the classical equations of motion with consideration of the size effects of micro-flow and microstructure, the in-plane and out-of-plane flexural vibrations of micro-scale pipes conveying fluid with clamped–clamped ends are examined theoretically by Wang et al. (2013). Focusing on the effects induced by different length ratios between the two segments, Dai et al. (2013) studied the dynamics of fluid-conveying cantilevered pipe consisting of two segments made of different materials. Li et al. (2014) described the fluid–structure interaction behavior of pipelines by considering the effects of pipe wall thickness, fluid pressure and velocity. Rahman and Alam (2012) investigated the vibration suppression of smart cantilever beams which consists of a beam as the host structure and piezoceramic patches as the actuation and sensing elements. Rathi and Khan (2012) used active vibration control and smart structure to reduce the vibration of a system by automatic modification of the system structural response.

In this paper an adaptive-robust control technique is proposed to suppress the vibration of a rotating cantilever pipe conveying fluid with a tip mass. The piezoelectric layers, which are attached to both sides of the pipe, are used as the sensors/actuators. The Lagrange method is used to derive the nonlinear coupled dynamic equations of the system and, as there is no simplification in the governing equations, these equations are complicated and nonlinear. The whole controlled dynamical system is simulated and the simulation results show the effectiveness of the control system.

Applying a modern control to suppress the vibration of a rotating cantilever pipe conveying fluid with tip mass by using the piezoelectric layers is the novelty of this study.

2 SYSTEM DYNAMICS

In this study a flexible cantilever pipe conveying fluid and a tip mass are assumed. Fig. 1 shows the schematic view of this pipe which connected to the rotating cylindrical hub.

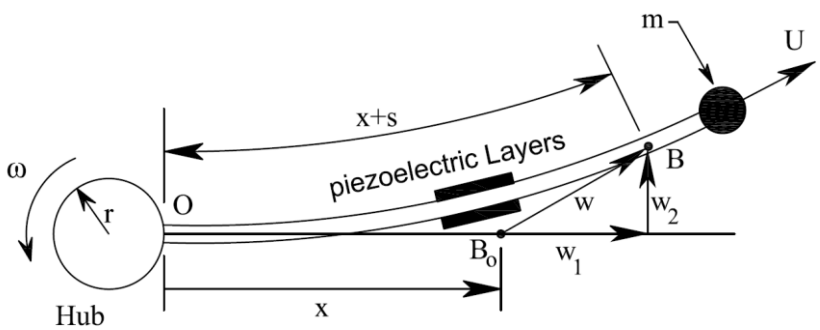

Figure 1. Schematic view of the rotating cantilever pipe.

The pipe is considered as a cantilever Euler-Bernoulli beam with length L, thickness h, radius r_b, density ρ, and Young's modulus E. The piezoelectric layers are attached to the pipe as sensors/actuators. Each piezoelectric layer has thickness h_p, density ρ_p, Young's modulus E_p and the equivalent piezoelectric coefficient e_{31}. The new position of point B_0 after deformation is the point B. W is the displacement vector of the point B_0 to B and has two components w_1 and w_2 which are axial and lateral deformation along the i and j axes, respectively. Also, m, U, and s are the magnitude of the tip mass, the velocity of the fluid flow, and the arc length stretch, respectively.

The governing equations of motion are derived base on the Lagrange method, which may be expressed as:

$$\frac{d}{dt}\left(\frac{\partial T}{\partial \dot{q}}\right)-\frac{\partial T}{\partial q}+\frac{\partial V}{\partial q}-\frac{\partial W_c}{\partial q}=Q_{nc} \tag{1}$$

where $V=V_p+V_f+V_{PZT}$ and $T=T_p+T_t+T_f+T_{PZT}$ are potential and kinetic energy, respectively. W_c is the work due to conservative external forces and Q_{nc} is the vector of generalized forces which is related to the non-conservative external forces. The subscripts p, f, PZT, and t stand for the pipe, fluid flow, piezoelectric layers, and tip mass, respectively.

2.1 Kinetic Energy of the System

For calculation of the kinetic energies, the velocities should be known. Consider the element B of the pipe; the velocity of this element can be determined as

$$\boldsymbol{v}_B = \boldsymbol{v}_0 + \boldsymbol{v}_{B/O} + \boldsymbol{\omega} \times (\boldsymbol{x} + \boldsymbol{w}) \tag{2}$$

where O is the base point of the pipe which is connected to the rotating hub and $\boldsymbol{v}_0$ is the velocity of this point. $\boldsymbol{v}_{B/O}$ is the relative velocity of element B with respect to the point O. $\boldsymbol{\omega}$ is the angular velocity of the hub, and $\boldsymbol{x}$ determine the position of the element before deflection. The parameters of Eq. (2) are expressed as follows:

$$\begin{aligned} \boldsymbol{v}_o &= r\omega\, j \\ \boldsymbol{v}_{B/O} &= \dot{w}_1 i + \dot{w}_2 j \\ \boldsymbol{\omega} &= \omega\, k \\ \boldsymbol{x} &= x\, i \\ \boldsymbol{w} &= w_1 i + w_2 j \end{aligned} \tag{3}$$

herein r is the radius of the hub and $(\dot{})$ illustrates the derivative with respect to time and i, j are the unit vectors. By substituting Eq. (3) in Eq. (2) the velocity of the point B can be determined as follows:

$$\boldsymbol{v}_B = (\dot{w}_1 - \omega w_2) i + (r\omega + \dot{w}_2 + \omega x + \omega w_1) j \tag{4}$$

If U is the relative velocity of fluid flow with respect to the pipe, the velocity vector of it will be

$$\boldsymbol{v}_f = U_x i + U_y j = \left\{ \dot{w}_1 - w_2\omega + U\left[1 - \frac{1}{2}\left(\frac{\partial w_2}{\partial x}\right)^2\right]\right\} i + \left\{ (r\omega + \dot{w}_2 + \omega x + \omega w_1) + U\frac{\partial w_2}{\partial x}\right\} j \tag{5}$$

Referring to the velocity vectors, the kinetic energies of the system are as follow

$$\begin{aligned} T_p &= \frac{1}{2}\rho \int_0^L (\boldsymbol{v}_B \boldsymbol{v}_B^T)\mathrm{d}x \\ T_t &= \frac{1}{2} m (\boldsymbol{v}_B \big|_{x=L})^2 \\ T_f &= \frac{1}{2} M_f \int_0^L (\boldsymbol{v}_f \boldsymbol{v}_f^T)\mathrm{d}x \\ T_{PZT} &= \frac{1}{2}\rho_p \sum_{n=1}^{N} \int_{PZT_n} (\boldsymbol{v}_B \boldsymbol{v}_B^T)\mathrm{d}x \end{aligned} \tag{6}$$

where N is the number of piezoelectric layers and M_f is the fluid mass per unit length of the pipe.

There is a geometric relation between arc length, s, and the Cartesian variables, w_1 and w_2, which can be used to substitute the variable s instead of w_1 in equations.

$$s \approx w_1 + \frac{1}{2}\int_0^x \left(\frac{\partial w_2}{\partial x}\right)^2 \mathrm{d}x \tag{7}$$

2.2 Work and Potential Energy of the System

The elastic energy of the pipe, which contains longitudinal and bending displacements, can be determined as:

$$V_p = \frac{1}{2}\int_0^L \left[EA_p\left(\frac{\partial s}{\partial x}\right)^2 + EI\left(\frac{\partial^2 w_2}{\partial x^2}\right)^2\right]\mathrm{d}x \tag{8}$$

The stress in piezoelectric layers can be expressed as (Fazelzadeh *el al.*, 2010)

$$\sigma_{x_{p_n}} = E_{p_n}\frac{\partial s}{\partial x} - E_{p_n} z\frac{\partial^2 w_2}{\partial x^2} - e_{31n}E_{z_n} \qquad n = 1\ldots N \tag{9}$$

where the subscript p_n represents the nth piezoelectric layer and $E_{z_n} = v_n/h_{p_n}$ $(n = 1\ldots N)$ is the electric field in the nth piezoelectric layer. v_n is the voltage which is related to the nth patch of piezoelectric layers. The first two terms on the right hand side of Eq. (9) are the stresses due to the mechanical effects and the last one is the stress due to electrical effect of the piezoelectric layers. Using Eq. (9) the potential energy of the piezoelectric layers is

$$\begin{aligned} V_{PZT} = {} & \frac{1}{2}\sum_{n=1}^{N}\int_{PZT_n} E_{p_n}\left(\frac{\partial s}{\partial x}\right)^2 \mathrm{d}v + \frac{1}{2}\sum_{n=1}^{N}\int_{PZT_n} E_{p_n} z^2\left(\frac{\partial^2 w_2}{\partial x^2}\right)^2 \mathrm{d}v + \\ & \frac{1}{2}\sum_{n=1}^{N}\int_{PZT_n} z e_{31}E_{z_n}\frac{\partial^2 w_2}{\partial x^2}\mathrm{d}v + \frac{1}{2}\sum_{n=1}^{N}\int_{PZT_n} E_{z_n} d_n \mathrm{d}v \end{aligned} \tag{10}$$

where z is the axis perpendicular to the piezoelectric surface, dv is a volumetric differential, and d_n is the electric displacement for the nth patch. The electric displacement is:

$$d_n = \varepsilon_{p_n}\frac{v_n}{h_p} \tag{11}$$

wherein ε_{p_n} is the dielectric constant of the piezoelectric material which forms the nth patch. The last term in Eq. (10) is the electric energy stored in the piezoelectric material.

The fluid discharge creates follower force that divided into two components. One is the conservative component of tangential follower force that creates conservative work that is given by

$$W_c = \frac{1}{2} M_f U^2 \int_0^L \left(\frac{\partial w_2}{\partial x} \right)^2 \mathrm{d}x \tag{12}$$

The other part is non-conservative force that creates non-conservative work δW_{nc}.

$$\delta W_{nc} = -M_f U \left(U \frac{\partial w_2}{\partial x} + \dot{w}_2 \right) \delta w_2 \Big|_{x=L} \tag{13}$$

2.3 Rayleigh–Ritz Formulation

Due to the intricacy of the governing equations, their solution may be achieved by an approximate solution procedure. To this end, w_2 and s can be represented by a series of trial shape functions, φ_{1_i} and φ_{2_i}, satisfying the boundary conditions, which each is multiplied by a time dependent generalized coordinate

$$\begin{aligned} s(x,t) &= \sum_{i=1}^{n} \varphi_{1i}(x) q_{1i}(t), \\ w_2(x,t) &= \sum_{i=1}^{n} \varphi_{2i}(x) q_{2i}(t), \end{aligned} \tag{14}$$

herein $q_{1i}(t)$ and $q_{2i}(t)$ are time dependent generalized coordinates and n is the number of mode shapes.

Substituting Eq. (14), instead of the parameters s and w_2, in above equations and using Eq. (1), the governing equations of motion are derived as:

$$\begin{aligned} &\begin{bmatrix} M_{11} & M_{12} \\ M_{21} & M_{22} \end{bmatrix} \begin{Bmatrix} \ddot{\mathbf{q}}_1 \\ \ddot{\mathbf{q}}_2 \end{Bmatrix} + \begin{bmatrix} C_{11} & C_{12} \\ C_{21} & C_{22} \end{bmatrix} \begin{Bmatrix} \dot{\mathbf{q}}_1 \\ \dot{\mathbf{q}}_2 \end{Bmatrix} + \begin{bmatrix} K_{11} & K_{12} \\ K_{21} & K_{22} \end{bmatrix} \begin{Bmatrix} \mathbf{q}_1 \\ \mathbf{q}_2 \end{Bmatrix} = \begin{Bmatrix} P_1 \\ P_2 \end{Bmatrix} - K_{pelaselect_a} \boldsymbol{v}_a \\ &\boldsymbol{v}_s = K^{-1}_{p_{elect}} K^T_{p_{elastelect_s}} \begin{Bmatrix} \mathbf{q}_1 \\ \mathbf{q}_2 \end{Bmatrix} \end{aligned} \tag{15}$$

where $\boldsymbol{v}_s$ and $\boldsymbol{v}_a$ are the sensors and actuators voltages, respectively. $K_{p_{elastelect_a}}$ and $K_{p_{elastelect_s}}$ denote the matrices of the elastic-electric effect of the piezoelectric actuator and sensor layers, respectively.

$$K_{p_{elastelect_a}} or \;\; K_{p_{elastelect_s}} = \begin{bmatrix} K_{pee_1} & K_{pee_2} & \cdots & K_{pee_N} \end{bmatrix} \tag{16}$$

where K_{pee_n} is the vector of the nth column of the elastic-electric matrix.

$$K_{pee_n} = \frac{e_{31n}}{h_{p_n}} \int_{PZT_n} \xi \frac{\partial^2 \boldsymbol{\Phi}}{\partial x^2} \mathrm{dv} \tag{17}$$

and $K_{p_{elect}}$ is a diagonal capacitance matrix of the piezoelectric patches (Azadi et al., 2015)

$$K_{p_{elect}} = \sum_{n=1}^{N} \int_{PZT_n} \varepsilon_{p_n} p_n p_n^T \mathrm{dv} \tag{18}$$

where the $N \times 1$ vector p_n has zero entries except for entry n which is equal to $1/h_{p_n}$. If the properties of all piezoelectric patches are the same, the capacitance matrix, $K_{p_{elect}}$, will be (Azadi et al., 2013)

$$K_{p_{elect}} = \varepsilon_p L_p b_p I_{N\times N} = \frac{1}{\mu} I_{N\times N} \tag{19}$$

herein $I_{N\times N}$ is the $N \times N$ identity matrix. The other parameters in Eq. (15) have been defined in appendix A.

3 ADAPTIVE-ROBUST CONTROLLER DESIGN

In this section, an adaptive-robust control algorithm is described to suppress the vibration of a rotating conveying fluid pipe. The proposed control method is a combination of adaptive and robust controllers, and so presents a useful controller in the presence of parameter uncertainties and disturbances. The possibility of on-line computation and decreasing the calculations are among the practical effective properties of the adaptive- robust controller.

The vector of the controller input is proposed to have the following form De et al. (1996)

$$v_a = K^{-1}_{p_{elastelect_a}} K_D \sigma - u_0 \tag{20}$$

K_D is a constant positive definite matrix, and

$$\dot{\xi} = -\Lambda \mathbf{q} \tag{21}$$

$$\sigma = \dot{\mathbf{q}} - \dot{\xi} = \dot{\mathbf{q}} - \Lambda \mathbf{q}$$

$$\mathbf{q} = \begin{Bmatrix} q_1 \\ q_2 \end{Bmatrix} \tag{22}$$

where Λ is a constant positive definite matrix and.

Equation (20), (15) and (22) give:

$$\begin{aligned} &M\dot{\sigma} + C\sigma + K_D\sigma = -M\ddot{\xi} - C\dot{\xi} - K\mathbf{q} + u_0 = \\ &-Y\eta + u_0 = w' + u_0 \end{aligned} \tag{23}$$

where

$$w' = Y\eta = M\ddot{\mathbf{q}} + C\dot{\mathbf{q}} + K\mathbf{q} \tag{24}$$

in which η is the vector of the estimated and exact base dynamic parameters of the system.

u_0 can be chosen as, Lewis et al. (1993):

$$u_0 = -\left(\beta^2 / (\varepsilon + \beta \|\sigma\|)\right)\sigma \tag{25}$$

where ε is a positive valued functions and β is a scalar that satisfy the following equation.

$$\left\| w' \right\| \le \beta \tag{26}$$

and from the properties above Lewis et al. (1993):

$$\begin{aligned} &\beta = \delta_0 + \delta_1 \left\| e \right\| + \delta_2 \left\| e \right\|^2 = \\ &[1 \quad \left\| e \right\| \quad \left\| e \right\|^2][\delta_0 \quad \delta_1 \quad \delta_2]^T = S\mu \end{aligned} \tag{27}$$

where $e = [\mathbf{q} \quad \dot{\mathbf{q}}]$, and the constant bounds δi's depend on K_D, Λ, k_c, k_k, k_m, k_M, $\hat{M}$, $\hat{C}$, and $\hat{K}$ and can be a priori calculated in a complicated and lengthy process (De et al., 1996). Herein k_m ($k_M < \infty$) denotes the strictly positive minimum (maximum) eigenvalue of M for all configurations of $\mathbf{q}$. k_C and k_K are some upper bounded positive constants for the C and K matrices. $S = [1 \quad \left\| e \right\| \quad \left\| e \right\|^2]$ is the coefficient vector of parameters.

Note that the equation (27) does not need to be changed, although the constant bounds do not have their previous values. These parameters can be updated by the following adaptation mechanism:

$$\dot{\hat{\mu}} = \dot{\tilde{\mu}} = -\gamma S^T \left\| \sigma \right\| \tag{28}$$

where γ is a positive definite matrix, $\tilde{\mu} = \hat{\mu} - \mu$, and $\hat{\beta}$ and $\tilde{\beta} = \hat{\beta} - \beta$ can be defined as:

$$\hat{\beta} = S\hat{\mu} \quad , \quad \tilde{\beta} = S\tilde{\mu} \tag{29}$$

The following Lyapunov function can be used for the stability analysis of the system:

$$V = \frac{\sigma^T M \sigma}{2} + \frac{\tilde{\mu}^T \gamma^{-1} \tilde{\mu}}{2} + K_\varepsilon^{-1} \varepsilon \tag{30}$$

where K_ε is a positive constant.

Taking the time derivative of equation (30) leads to:

$$\dot{V} = 1/2\, \sigma^T \dot{M}\, \sigma + \sigma^T M\, \dot{\sigma} + \tilde{\mu}^T \gamma^{-1} \dot{\tilde{\mu}} + k_\varepsilon^{-1} \dot{\varepsilon} \tag{31}$$

Substituting the control law (20) in the dynamic equations of the system leads to:

$$M\, \dot{\sigma} = -C\sigma - K_D \sigma + w' - u_o \tag{32}$$

By replacing equations (28) and (32) in equation (31) the following equation is obtained.

$$\begin{aligned} &\dot{V} = -\sigma^T K_D \sigma - S\tilde{\mu} \left\| \sigma \right\| + \sigma^T (w' - u_o) + \\ &k_\varepsilon^{-1} \dot{\varepsilon} + 1/2\, \sigma^T (\dot{M} - 2C)\sigma \end{aligned} \tag{33}$$

where the last term in equation (33) is equal to zero because of the skew symmetry property of $\dot{M} - 2C$ (De et al., 1996). With respect to the equations (26) and (27) we can show that:

$$\dot{V} \leq -\sigma^T K_D \sigma - S\tilde{\mu}\left\|\sigma\right\| + S\beta\left\|\sigma\right\| - \sigma^T u_o + k_\varepsilon^{-1}\dot{\varepsilon} \tag{34}$$

By assuming $\dot{\varepsilon} = -K_\varepsilon \varepsilon$ and substituting the equations (25) and (29) in equation (34), this equation can be simplified as:

$$\dot{V} \leq -\sigma^T K_D \sigma - \varepsilon + \frac{\varepsilon S\hat{\beta}\left\|\sigma\right\|}{S\hat{\beta}\left\|\sigma\right\| + \varepsilon} \tag{35}$$

As the summation of the two last terms in equation (35) is less than zero, the following non equality is produced.

$$\dot{V} < -\sigma^T K_D \sigma \tag{36}$$

Therefore, one may write:

$$\dot{V} \leq -\lambda_{\min}\left(K_D\right)\left\|\sigma\right\|^2 \tag{37}$$

where $\lambda_{\min}$ is the smallest eigenvalue of matrix K_D. This implies that:

$$V(0) - V(\infty) \geq \lambda_{\min}\int_0^\infty \left\|\sigma(t)\right\| \mathrm{d}t \tag{38}$$

Since $\dot{V}$ is negative semi-definite, it can be stated that V is a non-increasing function and, therefore, it is upper bounded by $V(0)$, then:

$$\lambda_{\min}\int_0^\infty \left\|r(\sigma)\right\| \mathrm{d}\sigma < \infty \tag{39}$$

or

$$\sqrt{\int_0^\infty \left\|\sigma(t)\right\|^2 \mathrm{d}t} < \infty \tag{40}$$

which shows $\sigma \in L_2^n$. To establish a stability result for the position error, one may write the transfer function relationship between the error and the filtered error, σ, as:

$$\mathbf{q}(s) = G(s).\sigma(s) = \left(sI + \Lambda\right)^{-1}.\sigma(s) \tag{41}$$

where s is the Laplace variable. Since $G\left(s\right)$ is a strictly proper, asymptotically stable transfer function and $\sigma \in L_2^\infty$, one may conclude that

$$\lim_{t\to\infty} \quad \mathbf{q} = 0 \tag{42}$$

Therefore, the position error, and also the velocity error asymptotically tend to zero.

4 SIMULATION RESULTS

In order to observe the response of the closed-loop control system and performance of the adaptive-robust controller, the governing equation of motion has been solved using Newmark integration method and the motion of the pipe is simulated. The parameters of the system are summarized in Table 1. The following family of functions for $\varphi_{1i}(x)$ and $\varphi_{2i}(x)$ used here, are defined as (Azadi et al., 2014):

$$\varphi_{1_i} \text{ and } \varphi_{2_i} = \frac{(x/L)^{1+i}\{6 + i^2(1 - x/L)^2 + i[5 - 6x/L + (x/L)^2]\}}{i(1+i)(2+i)(3+i)} \tag{43}$$

Length of pipe (m)	1
Out-radius of pipe (m)	0.025
In-radius of pipe (m)	0.02
Bending stiffness ($N \cdot m^2$)	8.9782
Density of pipe (kg/m^3)	2.766×10^3
Hub radius (m)	0.05

Table 1: Parameter values (Rougui et al., 2007).

The effects of the angular velocity of the pipe and the fluid velocity are studied. The simulation results are presented for four cases in which the angular velocities are $\omega = 1$ and 2 rad/s; and fluid velocities are $U = 0.5$ and 1 m/s. It is noteworthy to say that the pipe start to rotate from rest to a constant angular velocity, ω, during 8 seconds. To show the high performance of the controller algorithm, the controller gains are considered to be same for all four cases. The piezoelectric layer is attached to the middle of the pipe and is 0.2 m length. Fig. 2 compares the lateral tip deflection of the pipe with the results reported by Cai et al. (2004). Reasonable agreement between the present results and previous ones is seen. The transient time in this figure is considered to be 15 seconds. Figs. 3-6 show the lateral tip vibrations of the pipe. These figures illustrate that using piezoelectric actuator; the lateral tip vibrations of the pipe are suppressed rapidly. Although increasing the fluid velocity increase the amplitude of the vibrations, using piezoelectric actuator, the lateral vibration of the pipe is damped. Comparing Figs. 3 and 4, it is illustrated that by increasing the fluid flow velocity the transient tip deflection of the pipe increases approximately two times, but by applying the voltages to the piezoelectric actuator at the same time tip deflection is damped. It shows that the flow velocity has a little effect on the controller performance. Figs. 3-6 show that the effect of the increasing angular velocity on the transient lateral tip vibration is more than the effect of the fluid velocity, but in the steady state condition the effect of the flow velocity is more highlighted. The magnitude of the lateral generalized coordinates versus time is illustrated in Figs. 7-10. These magnitudes are presented for four mentioned cases. The behavior of the generalized coordinates is similar to the tip vibration of the pipe. Figs. 11-14 show the longitudinal vibrations of the tip of the pipe. Comparing Figs. 3-6 and 11-14 shows that although by applying the controller to the system the rate of decreasing the amplitude of the lateral and longitudinal vibrations of the pipe are approximately similar, but the lateral vibrations are damped more rapidly and the amplitude of these vibrations converge to zero during a short period of time. The time histories of the longitudinal generalized coordinates of the pipe are shown in Figs. 15-18.

Finally, Figs. 3-17 show the evidences of high effectiveness of the controller algorithm to suppress the flutter vibrations of the wing/store system.

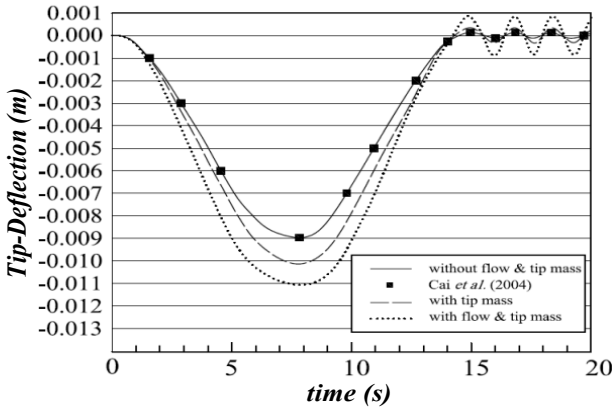

Figure 2: Validation of the pipe lateral tip vibrations ($U = 0.5$ m/s, $\omega = 1$ rad/s).

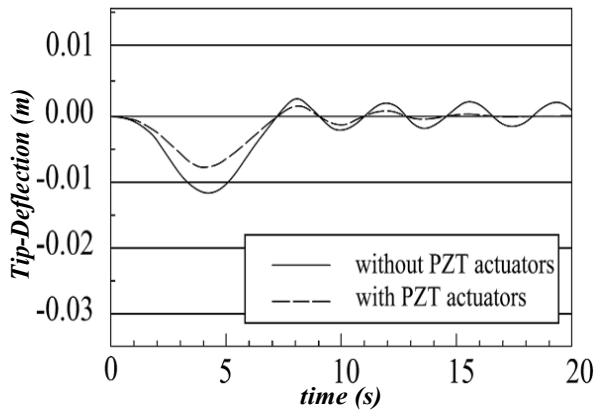

Figure 3: Latitude tip vibration of the Pipe ($U = 0.5$ m/s , $\omega = 1$ rad/s).

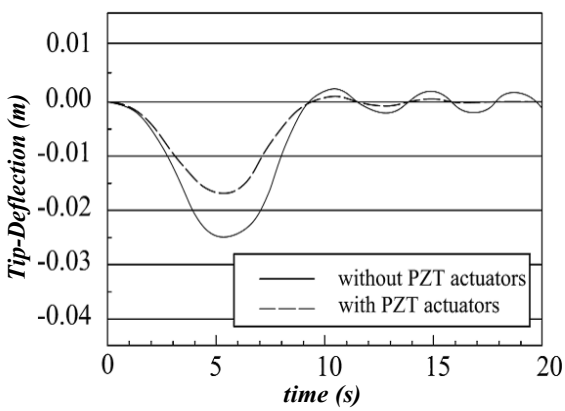

Figure 4: Latitude tip vibration of the Pipe ($U = 1$ m/s , $\omega = 1$ rad/s).

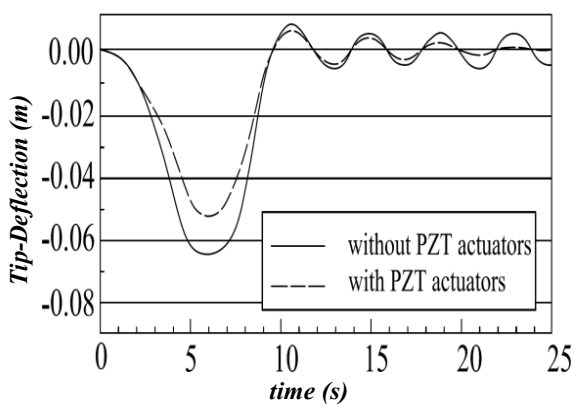

Figure 5: Latitude tip vibration of the Pipe ($U = 0.5$ m/s , $\omega = 2$ rad/s).

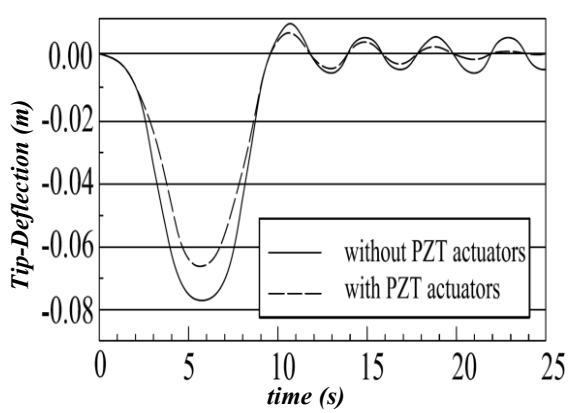

Figure 6: Latitude tip vibration of the Pipe ($U = 1$ m/s , $\omega = 2$ rad/s).

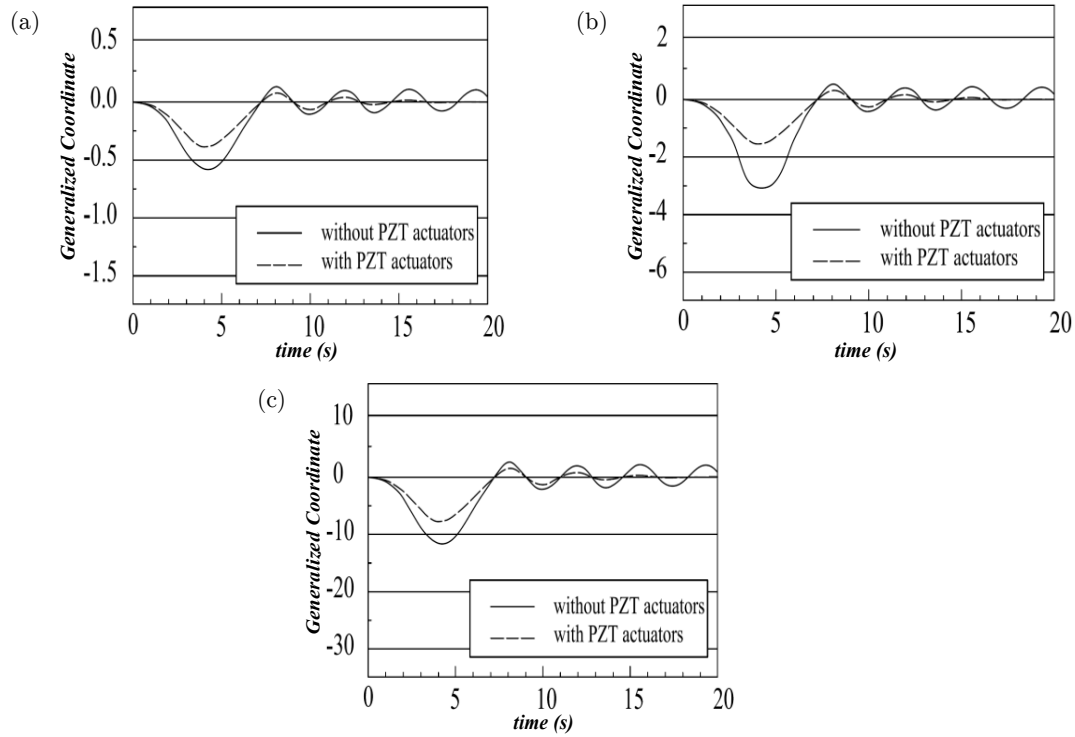

Figure 7: Time history of the lateral generalized coordinates of the pipe ($U = 0.5$ m/s , $\omega = 1$ rad/s): (a) First generalized coordinate (b) Second generalized coordinate (c) Third generalized coordinate.

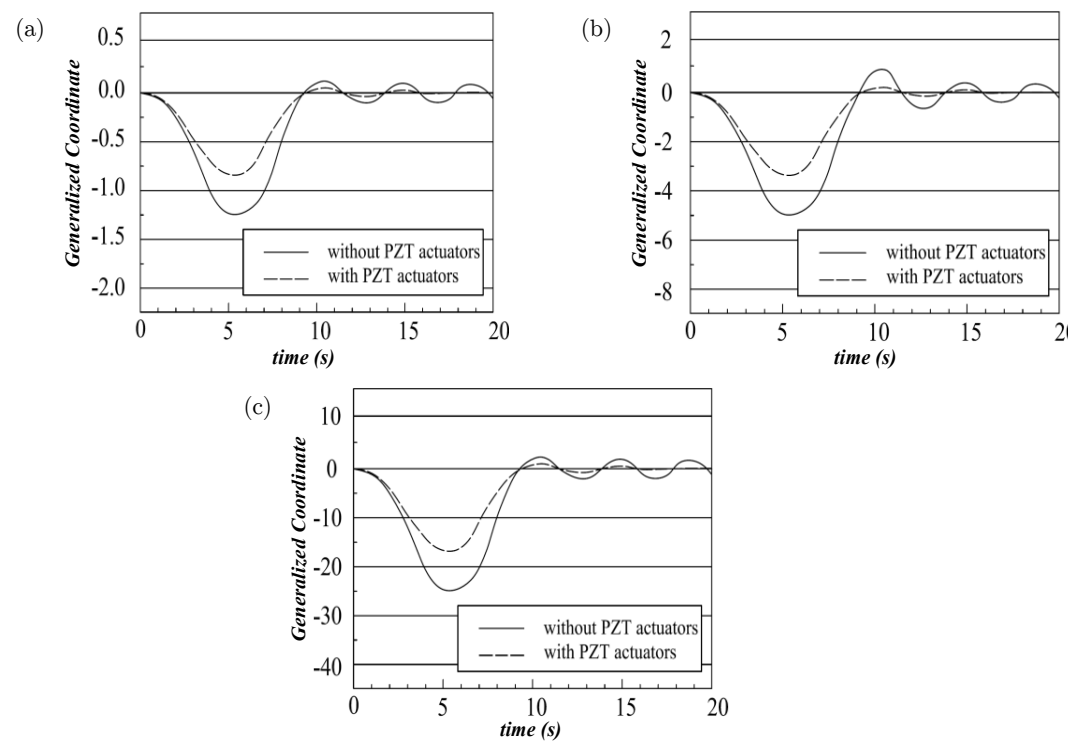

Figure 8: Time history of the lateral generalized coordinates of the pipe ($U = 1$ m/s , $\omega = 1$ rad/s): (a) First generalized coordinate (b) Second generalized coordinate (c) Third generalized coordinate.

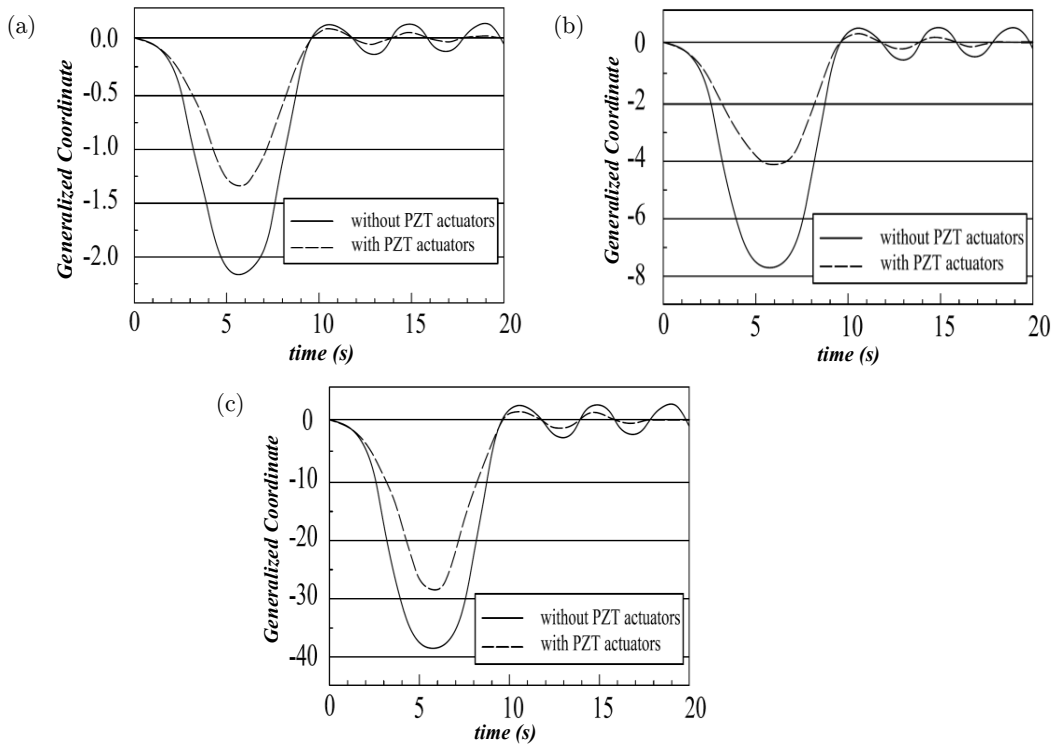

Figure 9. Time history of the lateral generalized coordinates of the pipe ($U = 0.5$ m/s , $\omega = 2$ rad/s): (a) First generalized coordinate (b) Second generalized coordinate (c) Third generalized coordinate.

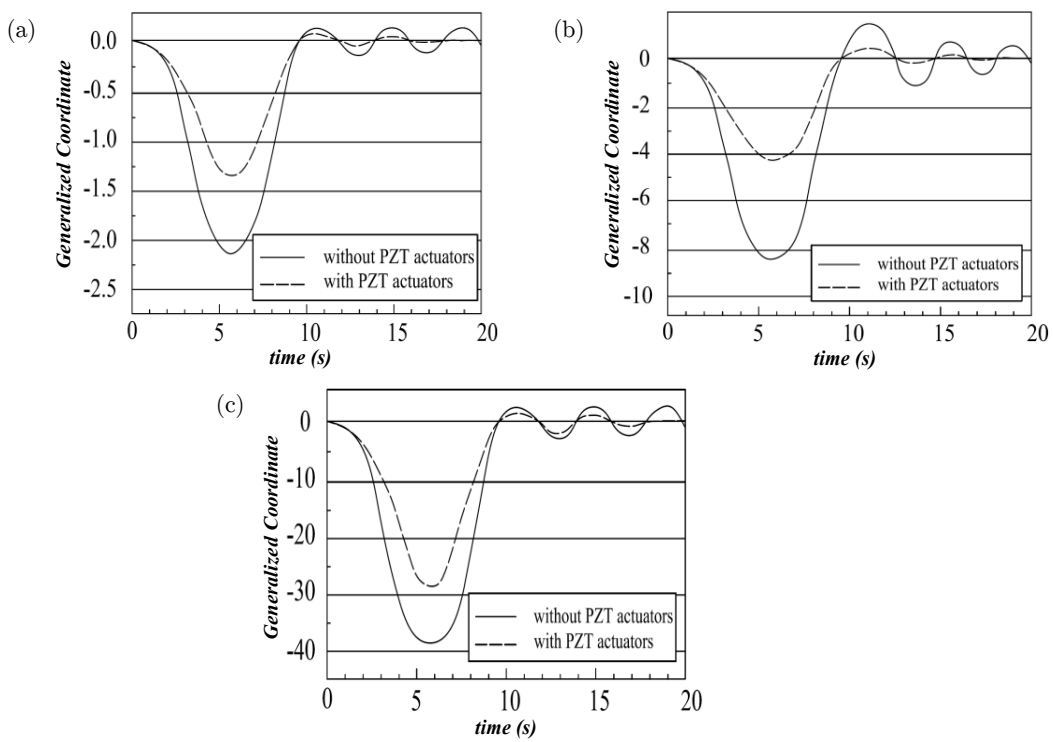

Figure 10: Time history of the lateral generalized coordinates of the pipe ($U = 1$ m/s , $\omega = 2$ rad/s): (a) First generalized coordinate (b) Second generalized coordinate (c) Third generalized coordinate.

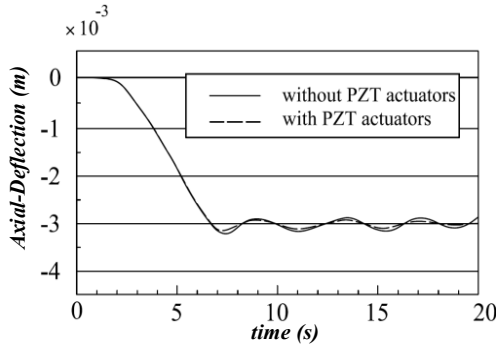

Figure 11: Longitudinal tip vibration of the pipe ($U = 0.5$ m/s , $\omega = 1$ rad/s).

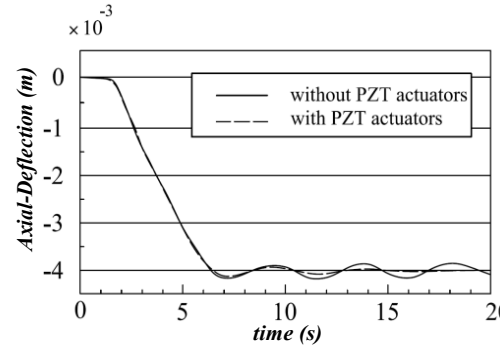

Figure 12: Longitudinal tip vibration of the pipe ($U = 1$ m/s , $\omega = 1$ rad/s).

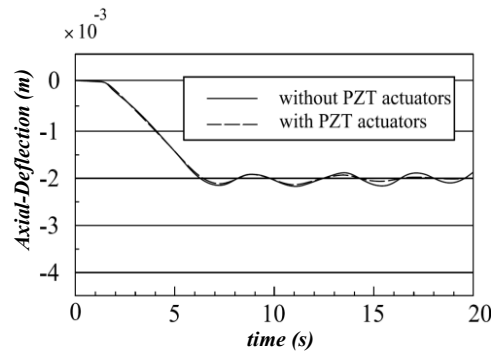

Figure 13: Longitudinal tip vibration of the pipe ($U = 0.5$ m/s , $\omega = 2$ rad/s).

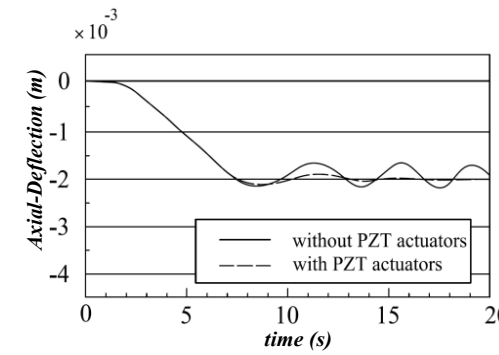

Figure 14: Longitudinal tip vibration of the pipe ($U = 1$ m/s , $\omega = 2$ rad/s).

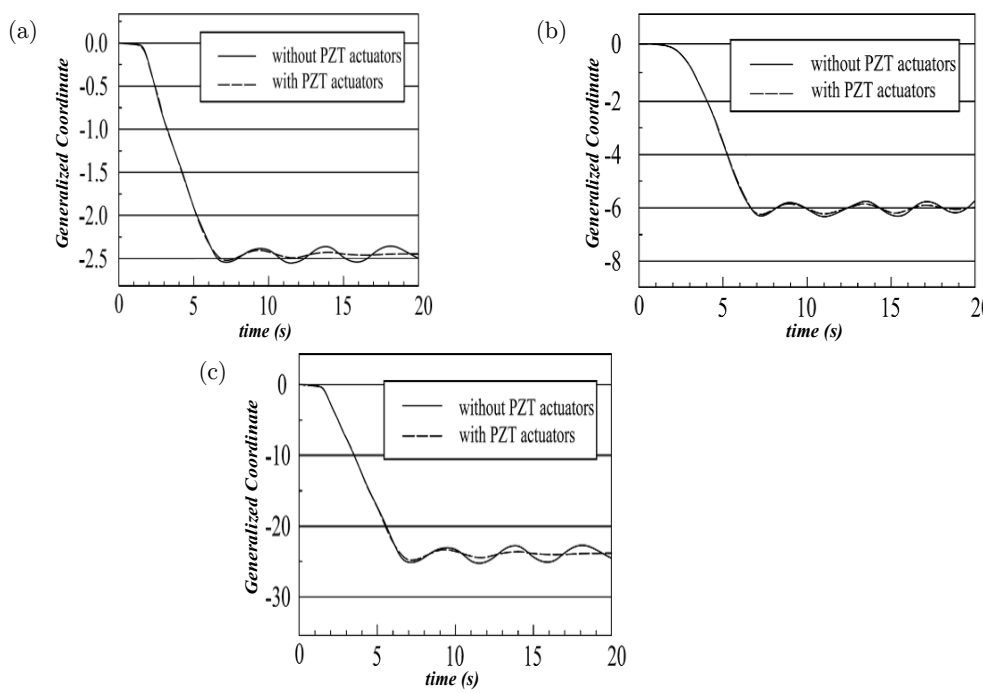

Figure 15: Time history of the longitudinal generalized coordinates of the pipe ($U = 0.5$ m/s , $\omega = 1$ rad/s): (a) First generalized coordinate (b) Second generalized coordinate (c) Third generalized coordinate.

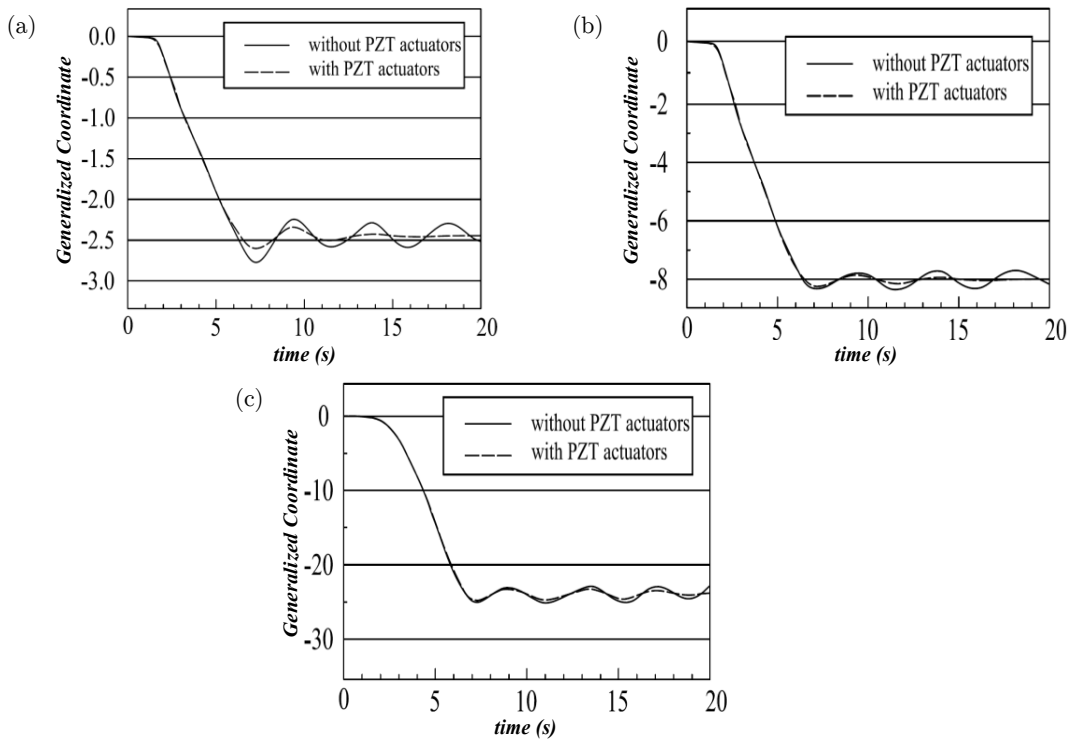

Figure 16: Time history of the longitudinal generalized coordinates of the pipe ($U = 1$ m/s , $\omega = 1$ rad/s): (a) First generalized coordinate (b) Second generalized coordinate (c) Third generalized coordinate.

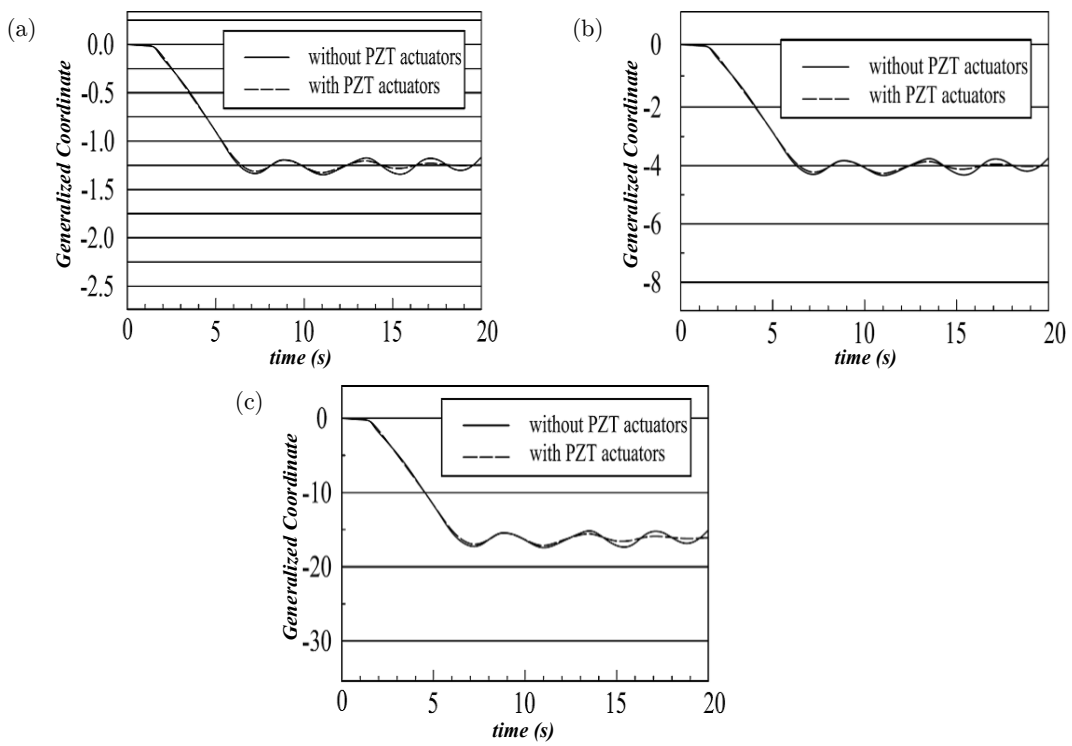

Figure 17: Time history of the longitudinal generalized coordinates of the pipe ($U = 0.5$ m/s , $\omega = 2$ rad/s): (a) First generalized coordinate (b) Second generalized coordinate (c) Third generalized coordinate.

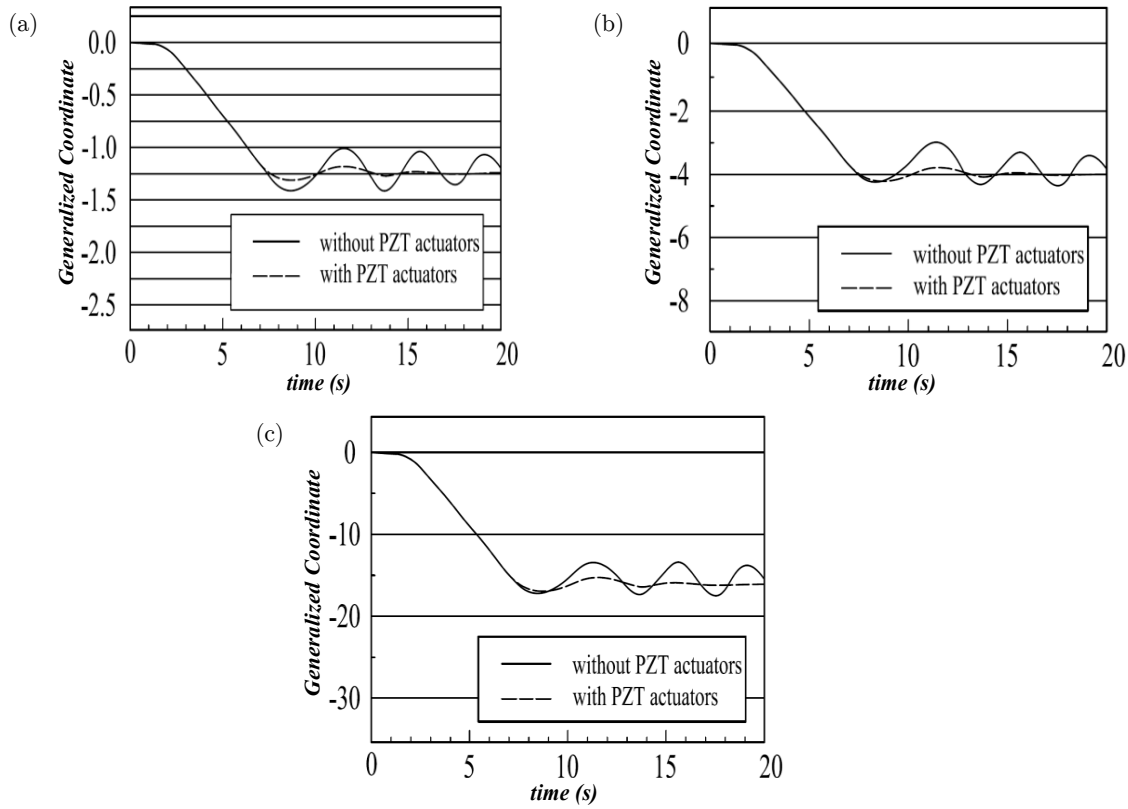

Figure 18: Time history of the longitudinal generalized coordinates of the pipe ($U = 1$ m/s , $\omega = 2$ rad/s): (a) First generalized coordinate (b) Second generalized coordinate (c) Third generalized coordinate.

5 CONCLUSIONS

In this study, the governing equations of motion of a rotating cantilever pipe conveying fluid have been derived, using Lagrange method. The pipe has been considered as an Euler-Bernoulli beam with tip mass. The piezoelectric layers have been attached both side of the pipe as sensor and actuator. The jet of the fluid cause a follower force applied to the pipe. The follower force and the rotation of the pipe induced the longitudinal and lateral vibrations to the system. An adaptive robust control scheme is applied to the system to suppress the lateral vibration of the pipe. The system is simulated and the effects of the angular velocity, and fluid flow on the lateral and longitudinal vibration of the system and the performance of the controller have been studied. The presented results showed that this controller is robust against different conditions.

References

Askari, E., Daneshmand, F., (2010). Coupled vibrations of cantilever cylindrical shells partially submerged in fluids with continuous, simply connected and non-convex domain. Journal of Sound and Vibration 329(17): 3520-3536.

Azadi, E., Eghtesad, M., Fazelzadeh, S.A., Azadi, M., (2013). Vibration suppression of smart nonlinear flexible appendages of a rotating satellite by using hybrid adaptive sliding mode/Lyapunov control. Journal of Vibration and Control 19(7): 975-991.

Azadi, M., Eghtesad, M., Fazelzadeh, S.A., Azadi, E., (2015). Dynamics and control of a smart flexible satellite moving in an orbit. Multibody Syst Dyn: DOI 10.1007/s11044-014-9447-2

Azadi, V., Azadi, M., Fazelzadeh, S.A., Azadi, E., (2014). Active control of a FGM beam under follower force with piezoelectric sensors/actuators. International Journal of Structural Stability and Dynamics 14: DOI: 10.1142/S0219455413500636

Chandiramani, N.K., (2010). Active control of a piezo-composite rotating beam using coupled plant dynamics. Journal of Sound and Vibration 329(14): 2716-2737.

Dai, H.L., Wang, L., Ni, Q., (2013). Dynamics of a fluid-conveying pipe composed of two different materials. International Journal of Engineering Science 73: 67-76.

De Wit, C.C., Siciliano, B., Bastin, G., (1996). Theory of robot control. Springer-Verlag New York, Inc.

Dzhupanov, V.A., Lilkova-Markova, S.V., (2003). Dynamic stability of a fluid-coveying cantilevered pipe on an additional combined support. International applied mechanics 39(2): 185-191.

Fazelzadeh, S.A., Eghtesad, M., Azadi, M., (2010). Buckling and flutter of a column enhanced by piezoelectric layers and lumped mass under a follower force. International Journal of Structural Stability and Dynamics 10(5): 1083-1097

Fung, E.H.K., Yau, D.T.W., (1999). Effects of centrifugal stiffening on the vibration frequencies of a constrained flexible arm. Journal of sound and vibration 224(5): 809-841.

Fung, E.H.K., Yau, D.T.W., (2004). Vibration characteristics of a rotating flexible arm with ACLD treatment. Journal of Sound and Vibration 269(1): 165-182.

Ghayesh, M.H., Païdoussis, M.P., Amabili, M., (2013). Nonlinear dynamics of cantilevered extensible pipes conveying fluid. Journal of Sound and Vibration 332(24): 6405-6418.

Hellum, A., Mukherjee, R., Hull, A.J., (2011). Flutter instability of a fluid-conveying fluid-immersed pipe affixed to a rigid body. Journal of Fluids and Structures 27(7): 1086-1096.

Langthjem, M.A., Sugiyama, Y., (1999). Vibration and stability analysis of cantilevered two-pipe systems conveying different fluids. Journal of fluids and structures 13(2): 251-268.

Lewis, F.L., Abdallah, C.T., Dawson, D.M., (1993). Control of robot manipulators. Vol. 236. New York: Macmillan.

Li, S., Liu, G., Kong, W., (2014). Vibration analysis of pipes conveying fluid by transfer matrix method. Nuclear Engineering and Design 266: 78-88.

Lim, J.-H., Jung, G.-C., Choi, Y.-S., (2003). Nonlinear dynamic analysis of cantilever tube conveying fluid with system identification. KSME international journal 17(12): 1994-2003.

Lin, W., Qiao, N., (2008). Vibration and Stability of an Axially Moving Beam Immersed in Fluid. International journal of solids and structures 45: 1445-1457.

Païdoussis, M.P., Semler, C., Wadham-Gagnon, M., Saaid, S., (2007). Dynamics of cantilevered pipes conveying fluid. Part 2: dynamics of the system with intermediate spring support. Journal of Fluids and Structures 23(4): 569-587.

Rahman, N., Alam, M.N., (2012). Active vibration control of a piezoelectric beam using PID controller: Experimental study. Latin American Journal of Solids and Structures 9(6): 657-673.

Rathi, V., Khan, A.H., (2012). Vibration attenuation and shape control of surface mounted, embedded smart beam. Latin American Journal of Solids and Structures 9(3): 1-25.

Rinaldi, S., Païdoussis, M.P., (2010). Dynamics of a cantilevered pipe discharging fluid, fitted with a stabilizing end-piece. Journal of Fluids and Structures 26(3): 517-525.

Rougui, M., Moussaoui, F., Benamar, R., (2007). Geometrically Non-Linear Free and Forced Vibration of Simply Supported Circular Cylindrical Shells: A Semi-Analytical Aproach. International journal of non-linear mechanics 42: 1102-1115.

Wadham-Gagnon, M., Semler, C., (2007). Dynamics of cantilevered pipes conveying fluid. Part 1: Nonlinear equations of three-dimensional motion. Journal of fluids and structures 23(4): 545-567.

Wang, L., Dai, H.L., (2012). Vibration and enhanced stability properties of fluid-conveying pipes with two symmetric elbows fitted at downstream end. Archive of Applied Mechanics 82(2): 155-161.

Wang, L., Liu, H.T., Ni, Q., Wu, Y., (2013). Flexural vibrations of microscale pipes conveying fluid by considering the size effects of micro-flow and micro-structure. International Journal of Engineering Science 71: 92-101.

Wang, Y., Guo, X.H., Li, Y.G., Li, J., (2010a). Nonlinear Traveling Wave Vibration of a Circular Cylindrical Shell Subject to a Moving Concentrated Harmonic Force. Journal of sound and vibration 329: 338-352.

Wang, Y.Q., Guo, X.H., Chang, H.H., Li, H.Y., (2010b). Nonlinear dynamic response of rotating circular cylindrical shells with precession of vibrating shape—Part I: Numerical solution. International Journal of Mechanical Sciences 52(9): 1217-1224.

Yoon, H.-I., Son, I.-S., (2006). Dynamic behavior of cracked simply supported pipe conveying fluid with moving mass. Journal of sound and vibration 292(3): 941-953.

Yoon, H.-I., Son, I.-S., (2007). Dynamic response of rotating flexible cantilever pipe conveying fluid with tip mass. International journal of mechanical sciences 49(7): 878-887.

Appendix A

$$
\begin{aligned}
M &= \begin{bmatrix} M_{11} & M_{12} \\ M_{21} & M_{22} \end{bmatrix} \\
M_{11} &= \rho \int_{Pipe} \phi_{1i}\phi_{1j}\mathrm{d}x + \rho_{PZT} \int_{PZT} \phi_{1i}\phi_{1j}\mathrm{d}x + M_f \int_{Pipe} \phi_{1i}\phi_{1j}\mathrm{d}x + m\phi_{1Li}\phi_{1Lj} \\
M_{22} &= \rho \int_{Pipe} \phi_{2i}\phi_{2j}\mathrm{d}x + \rho_{PZT} \int_{PZT} \phi_{2i}\phi_{2j}\mathrm{d}x + M_f \int_{Pipe} \phi_{2i}\phi_{2j}\mathrm{d}x + m\phi_{2Li}\phi_{2Lj} \\
M_{12} &= M_{21} = 0
\end{aligned}
\tag{A1}
$$

$$
\begin{aligned}
C &= \begin{bmatrix} C_{11} & C_{12} \\ C_{21} & C_{22} \end{bmatrix} \\
C_{11} &= C_{22} = 0 \\
C_{12} &= -2\rho\Omega \int_{Pipe} \phi_{1i}\phi_{2j}\mathrm{d}x - 2\rho_{PZT}\Omega \int_{PZT} \phi_{1i}\phi_{2j}\mathrm{d}x - 2M_f\Omega \int_{Pipe} \phi_{1i}\phi_{2j}\mathrm{d}x - 2m\Omega\phi_{1Li}\phi_{2Lj} - \\
&\qquad M_f U \sum_k \left(q_{2k} \int_{Pipe} \phi_{1i} \frac{\partial\phi_{2j}}{\partial x} \frac{\partial\phi_{2k}}{\partial x} \mathrm{d}x \right) \\
C_{21} &= 2\rho\Omega \int_{Pipe} \phi_{1i}\phi_{2j}\mathrm{d}x + 2\rho_{PZT}\Omega \int_{PZT} \phi_{1i}\phi_{2j}\mathrm{d}x + 2M_f\Omega \int_{Pipe} \phi_{1i}\phi_{2j}\mathrm{d}x + 2m\Omega\phi_{1Li}\phi_{2Lj} + \\
&\qquad M_f U \sum_k \left(q_{2k} \int_{Pipe} \phi_{1i} \frac{\partial\phi_{2j}}{\partial x} \frac{\partial\phi_{2k}}{\partial x} \mathrm{d}x \right)
\end{aligned}
\tag{A2}
$$

$$K = \begin{bmatrix} K_{11} & K_{12} \\ K_{21} & K_{22} \end{bmatrix}$$

$$K_{11} = \rho\Omega^2 \int_{Pipe} \phi_{1i}\phi_{1j}\mathrm{d}x + \rho_{PZT}\Omega^2 \int_{PZT} \phi_{1i}\phi_{1j}\mathrm{d}x + M_f\Omega^2 \int_{Pipe} \phi_{1i}\phi_{1j}\mathrm{d}x + m\Omega^2\phi_{1Li}\phi_{1Lj} + EA\int_{Pipe} \frac{\partial\phi_{1i}}{\partial x}\frac{\partial\phi_{1j}}{\partial x}\mathrm{d}x$$

$$K_{12} = M_f\Omega U \int_{Pipe} \phi_{1i}\frac{\partial\phi_{2j}}{\partial x}\mathrm{d}x + \rho\dot{\Omega}\int \phi_{1i}\phi_{2j}\mathrm{d}x + \rho_{PZT}\dot{\Omega}\int \phi_{1i}\phi_{2j}\mathrm{d}x + M_f\dot{\Omega}\int \phi_{1i}\phi_{2j}\mathrm{d}x + m\dot{\Omega}\phi_{1Li}\phi_{2Lj}$$

$$K_{21} = M_f\Omega U \int_{Pipe} \phi_{1j}\frac{\partial\phi_{2i}}{\partial x}\mathrm{d}x + \rho\dot{\Omega}\int \phi_{1i}\phi_{2j}\mathrm{d}x + \rho_{PZT}\dot{\Omega}\int \phi_{1i}\phi_{2j}\mathrm{d}x + M_f\dot{\Omega}\int \phi_{1i}\phi_{2j}\mathrm{d}x + m\dot{\Omega}\phi_{1Li}\phi_{2Lj} \tag{A3}$$

$$K_{22} = \rho\Omega^2 \int_{Pipe} \phi_{2i}\phi_{2j}\mathrm{d}x + \rho_{PZT}\Omega^2 \int_{PZT} \phi_{2i}\phi_{2j}\mathrm{d}x + M_f\Omega^2 \int_{Pipe} \phi_{2i}\phi_{2j}\mathrm{d}x + m\Omega^2\phi_{2Li}\phi_{2Lj} +$$
$$3U\Omega\sum_k q_{2k}\int_{Pipe} \phi_{2i}\frac{\partial\phi_{2j}}{\partial x}\frac{\partial\phi_{2k}}{\partial x}\mathrm{d}x + \frac{3}{2}U^2\sum_k\sum_l q_{2k}q_{2l}\int_{Pipe} \frac{\partial\phi_{2i}}{\partial x}\frac{\partial\phi_{2j}}{\partial x}\frac{\partial\phi_{2k}}{\partial x}\frac{\partial\phi_{2l}}{\partial x}\mathrm{d}x + \Omega U\int_{Pipe} \phi_{1j}\frac{\partial\phi_{2i}}{\partial x}\mathrm{d}x +$$
$$EI\int_{Pipe} \frac{\partial^2\phi_{2i}}{\partial x^2}\frac{\partial^2\phi_{2j}}{\partial x^2}\mathrm{d}x + M_fU^2\int_{Pipe} \frac{\partial\phi_{2i}}{\partial x}\frac{\partial\phi_{2j}}{\partial x}\mathrm{d}x$$

$$P_1 = \rho r\Omega^2\int \phi_{1i}\mathrm{d}x + \rho_{PZT}r\Omega^2\int_{PZT} \phi_{1i}\mathrm{d}x + M_f r\Omega^2\int \phi_{1i}\mathrm{d}x + mr\Omega^2\phi_{1L} + \rho\Omega^2\int x\phi_{1i}\mathrm{d}x +$$
$$\rho_{PZT}\Omega^2\int_{PZT} x\phi_{1i}\mathrm{d}x + M_f\Omega^2\int x\phi_{1i}\mathrm{d}x + m\Omega^2L\phi_{1L} \tag{A4}$$
$$P_2 = -M_fU\Omega\int \phi_{2i}\mathrm{d}x + M_fUr\Omega\int \frac{\partial\phi_{2i}}{\partial x}\mathrm{d}x + M_fU\Omega\int x\frac{\partial\phi_{2i}}{\partial x}\mathrm{d}x$$